

A Design of Low-pass Filter with Wide Stopband and Sharp Roll-off Rate Using Series LC Tanks Resonator

A. R. Nouritabar, Ashkan Abdipour, and Arash Abdipour

Young Researchers and Elite Club, Kermanshah Branch, Islamic Azad University, Kermanshah, Iran
Alireza.Nouritabar@yahoo.com, Ashkan_Abdipour@yahoo.com, Arash.Abdipour@yahoo.com

Abstract — In this letter, a lowpass filter (LPF) using resonators synthesized with series LC tank patches has been proposed. Each of the employed LC tank is composed of a high-low impedance lines, which have been mirrored to create the patches of the main resonance cells. Using this kind of resonator combining with eight suppressing cells leads to designing a LPF with specifications such as ultra-wide stopband, sharp cut-off and an acceptable return loss in the pass band. The -3 dB cut-off frequency of the proposed LPF is located in 2.4 GHz. The spurious frequencies have been suppressed in the stop-band region from 2.66 up to 23 GHz with a suppression level of -35 dB. Moreover, the transition band has been measured from 2.4 to 2.67 GHz with corresponding attenuation levels of -3 and -40 dB, respectively. To clarify the performance of each section and how they affect the frequency response the equivalent LC circuit of resonators and the final design have been obtained, separately.

Index Terms — High-low impedance lines, LC tank patches, Lowpass Filter (LPF).

I. INTRODUCTION

Microstrip LPFs are one of the most important components that have been utilized widely in wireless communication systems and played a key role for many years. So far, several compact LPFs have been proposed to achieve a desired frequency response such as wide stopband with high rejection level and sharp roll-off. For example, in [1], a microstrip lowpass filter with quasi-elliptic response using both loaded radial-shape patches and meandered main transmission line has been proposed. However, it suffers from a gradual transition band and low level of stopband rejection. To expand the stopband region in the frequency response of LPFs, hairpin resonators can be useful [2-6]. By utilizing this unit in [2], the stopband has been expanded. However, the overall circuit size is relatively large and the skirt performance is not desired. A method to design a LPF with wide stopband is using stepped impedance hairpin resonator with radial stubs, which has been done in [3], but this design has been failed to

achieve a sharp roll-off rate. In [4], by employing stepped impedance hairpin units a compact LPF has been proposed. However, this filter has a narrow stopband. In [5], another method to propose a LPF based on an application of shunt open-stubs coupled-line in the structure of hairpin unit has been introduced. It has retained a wide stopband as the main characteristic of hairpin resonators. A gradual transition band and large circuit size have been remained significant challenges, though. In [6], defected ground structure (DGS) as a popular method is applied to design a LPF with sharp rejection. However, DGS increases the complexity of design procedure and the proposed circuit using this method cannot be utilized on metal surfaces. To design a LPF rat-race directional couplers have been used to operate as bandstop transversal filtering sections (TFSs), in [7]. However, by adopting this method the occupied area has been significantly increased and also the rejection band has not been adequately widened. In [8], a quasi- π -slot resonator and open stubs is employed and a LPF with sharp transition band is proposed, but the occupied area is relatively large. A microstrip LPF by using triangular and radial patch resonators has been designed [9], but this filter suffers from gradual transition band. In this letter, a lowpass filter (LPF) with -3 dB cut-off frequency located on 2.4 GHz has been proposed. The designed LPF is composed of a main resonator with series LC tank patches and complete resonance cells having the same structure as the main one to omit the aforementioned defects of the frequency response. To expand the stopband more, eight suppressing cells have been employed in both sides of the proposed LPF.

II. THE PROCEDURE OF DESIGNING THE PROPOSED LPF

To define the basic structure of series LC tanks configuration, Fig. 1 (a) shows the primary resonance cell using these patches. As it is observed, the designed resonator consists of two high-low impedance transmission lines standing for LC tank patches. The dimensions of the implemented resonator are as follows: $L1 = 2.9$, $L2 = 3.1$, $L3 = 0.75$, $W1 = W2 = W3 = 0.1$,

$W4 = 21.5$, $W5 = 20.5$, $S1 = 0.3$ (all in millimetre). In Fig. 1 (b) the frequency response of the resonator has been shown. For the simulation, Agilent Advanced Design System (ADS) is used.

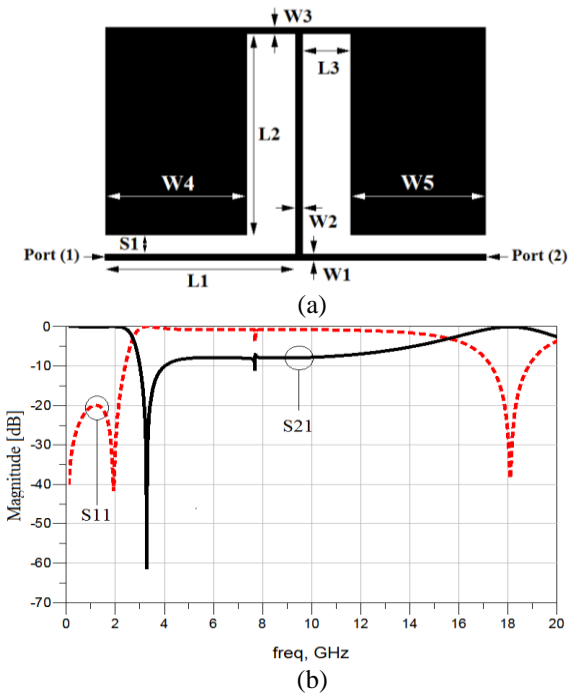


Fig. 1. (a) The basic structure of series LC tanks configuration, and (b) frequency response of the basic structure of series LC tanks configuration.

As it can be seen from the S-parameters, the operating frequency of this resonance cell is located on 2.4 GHz. According to the simulation results, the insertion and return losses in the pass band are 0.1 and rather greater than +20 dB, respectively. Moreover, the proposed cell creates a transition zero at 3.3 GHz with corresponding attenuation level of -61 dB bringing about a wide suppressing band of -7 dB. By changing the dimensions of the mentioned resonance cell the location of -3 dB operating frequency and also the transition zero can be controlled. To justify how it is possible, the simulated frequency response of the designed resonator against $L2$ and $W2$ is shown in Figs. 2 (a) and (b), respectively. As it is observed from Fig. 2 (a), by decreasing $L2$ from 3.1 to 2.3 mm with steps of 0.4 mm, because of reducing the value of capacitance of the low impedance line, the transmission zero in 3.3 GHz will move away from the lower frequencies. Similarly, in Fig. 2 (b), when $W2$ increases from 0.1 to 0.3 mm with steps of 0.1 mm, transmission zero will

close to the upper frequency. Hence, the location of the transmission zero can be controlled by changing the length of $L2$ and the width of $W2$.

The equivalent LC circuit of the proposed cell and a comparison between the frequency responses of LC circuit and EM simulations have been shown in Figs. 3 (a) and (b), respectively. In the lumped circuit $L1$ and $L2$ represent the inductances of the transmission lines determined by $W1$ and $W2$, in Fig. 1 (a). $L3$, $C4$ and $C5$ model the inductance and capacitance of LC tank patch. $C1$, $C2$ and $C3$ account for the capacitance between the microstrip structure and the ground.

The values of inductances and capacitances are $L1 = 2.9$ nH, $L2 = 3.4$ nH, $L3 = 0.75$ nH, $C1 = 37$ fF, $C2 = 80$ fF, $C3 = 63$ fF, $C4 = 0.29$ pF, $C5 = 0.28$ pF. Figure 4 indicates the main resonator utilizing primary resonance cell with series LC tanks patches where each of the employed primary resonance cell has the same dimension of that shown in Fig. 1 (a). As it is observed, two of the primary cells are placed on the both sides of the main transmission line. In Fig. 5, the frequency response of this resonator is illustrated.

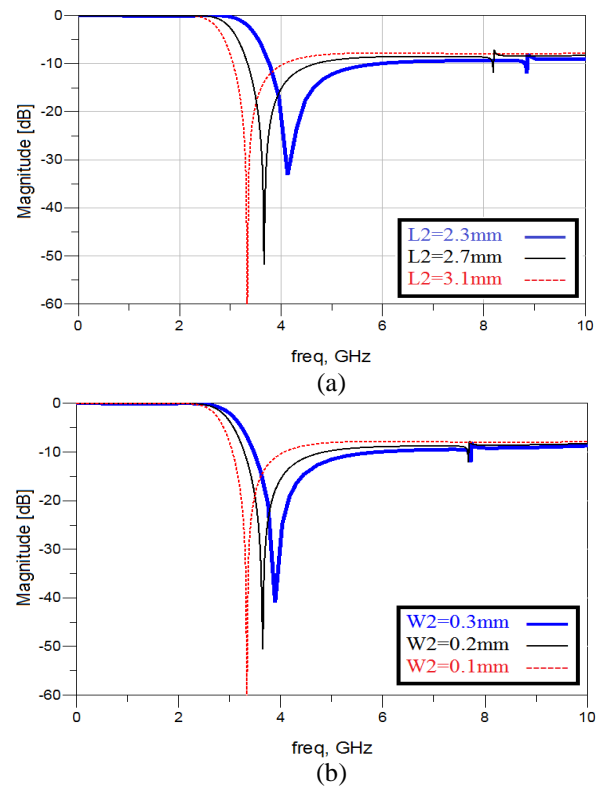


Fig. 2. (a) Magnitude of S_{21} versus changing the value of $L2$, and (b) magnitude of S_{21} versus changing the value of $W2$.

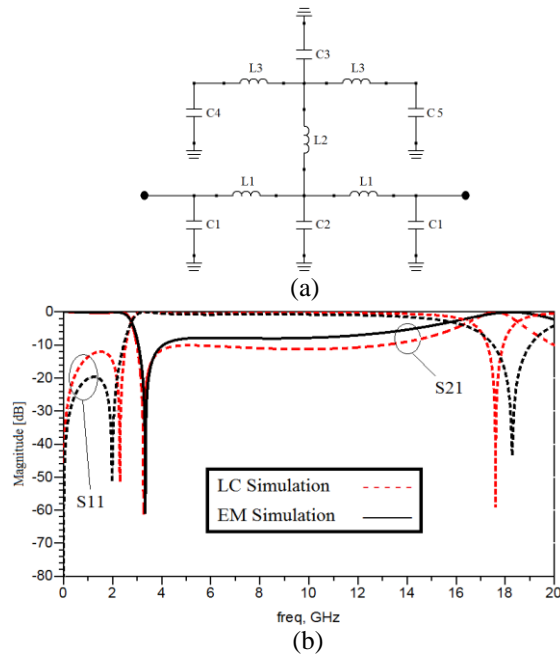


Fig. 3. (a) The equivalent LC circuit of the shown basic structure in Fig. 1 (a), and (b) the comparison between the frequency responses of LC circuit and EM simulations.

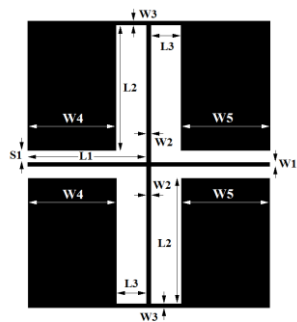


Fig. 4. The structure of the main resonator with the same dimensions as that shown in Fig. 1 (a).

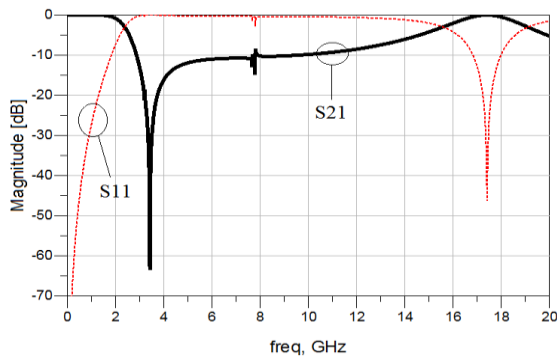


Fig. 5. The frequency response of the main resonator shown in Fig. 4.

According to the scattering parameters of the proposed resonator, it suffers from a low level of suppression in the whole stopband and a gradual transition band. To create some transmission zeros (TZs), several stages of the proposed resonator with different dimensions can be connected in series. The applied resonators to complete the operation of the main resonator are so-called complete resonance cells (S-CCRCs). Creating TZs at different frequencies not only improves the suppressing level of the rejection band but also leads to expanding the stopband region. However, setting several resonators in series increases the coupling effects, which causes to destroy the insertion loss in the passband region. Note that, the dimensions of S-CCRC must be chosen to achieve a higher -3 dB operating frequency than the main resonator having 2.4 GHz cut-off frequency, the lowest suppression in the pass band (to have no effect on the pass band of the main resonator) and high and wide stopband. The structure of S-CCRC having different dimensions in comparison to that shown in Fig. 4 and its equivalent LC circuit have been depicted in Figs. 6 (a) and (b), respectively. The dimensions of S-CCR are as follows: $L4 = 2.3$, $L5 = 3$, $L6 = 0.4$, $W6 = 0.1$, $W7 = 0.1$, $W8 = 0.1$, $W9 = 1.9$ and $S2 = 0.3$ (all in millimeter). The values of lumped elements are as follows: $L4 = 1.66$ nH, $L5 = 2.45$ nH, $L6 = 0.3$ nH, $C6 = 30$ fF, $C7 = 104$ fF, $C8 = 63$ fF, $C9 = 0.32$ pF. Actually, the proposed S-CCR has been designed to eliminate the defects of the frequency response of the main resonator. Figure 7 illustrates the frequency responses of LC circuit and EM simulation of S-CCR.

As shown in Figs. 8 (a) and (b) ($S4 = 0.2$ mm, $S3 = 0.2$ mm), by connecting two of S-CCRCs and the main resonator (see Fig. 8 (a)), the mentioned intents such as desired return loss (about +17 dB) and insertion loss (close to 0.1 dB) in whole pass band have been obtained. Moreover, the transition band from -3 up to -40 dB is 0.27 GHz and also, to some extent, an improved stopband is achieved.

Although the rejection band has been broadened, undesired poles over the frequency of 11 GHz do not let it to be expanded enough. To widen the stopband four high-low impedance resonators as suppressing cells are employed. The configuration of these cells and corresponding equivalent LC circuit are shown in Figs. 9 (a) and (b), respectively. In the LC circuit $L7, L8, L9, L10$ and $L11$ are the equivalent inductors of the transmission lines determined by $L7, L8, L9, L10$ and $L11$ in Fig. 9 (a). $C10, C11, C12, C13$ and $C14$ model the capacitance between the microstrip structure and the ground. $C15$ and $C16$ present the equivalent capacitances of the open stubs determined by $L12$ in the microstrip structure of suppressing cells. The coupling effects of two adjacent rectangular low impedance patches have been modeled by $Cg1$.

The dimensions of the proposed suppressing cell are: $W_{10} = 0.3$, $L_{11} = 0.2$, $L_{10} = 3.2$, $L_9 = 1.25$, $L_8 = 2.1$, $L_7 = 1$, $W_{16} = 1.1$, $W_{15} = 0.1$, $W_{14} = 0.95$, $W_{13} = 1$, $W_{12} = 0.1$, $W_{11} = 0.1$ (all in millimetre), and the values of capacitances and inductors are as: $L_7 = 0.48$ nH, $L_8 = 0.132$ nH, $L_9 = 1.39$ nH, $L_{10} = 0.833$ nH, $L_{11} = 0.2$ nH, $C_{10} = 17$ fF, $C_{11} = 20$ fF, $C_{12} = 32$ fF, $C_{13} = 44$ fF, $C_{14} = 15$ fF, $C_{15} = 0.332$ pF, $C_{16} = 0.35$ pF, $C_{g1} = 75$ fF.

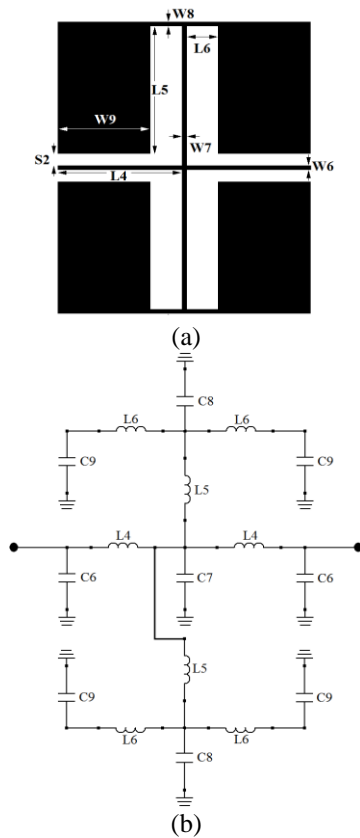


Fig. 6. (a) The configuration of complete resonance cells (S-CCRCs), and (b) the LC circuit of the complete resonance cells (S-CCRCs).

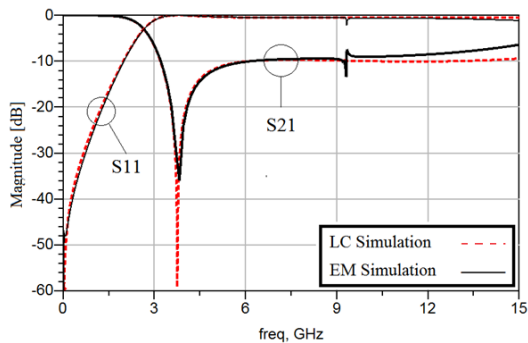


Fig. 7. The comparison between the frequency responses of LC circuit and EM simulations of S-CCRC.

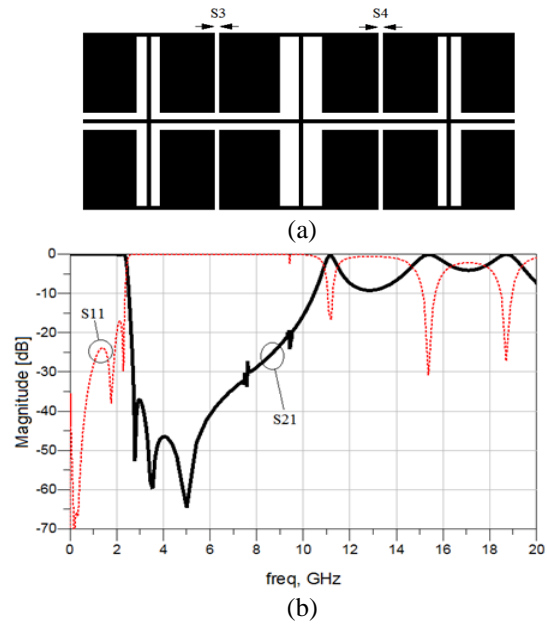


Fig. 8. (a) The configuration of connecting two of S-CCRCs and the main resonator, and (b) the frequency response of connecting two out of S-CCRCs and the main resonator.

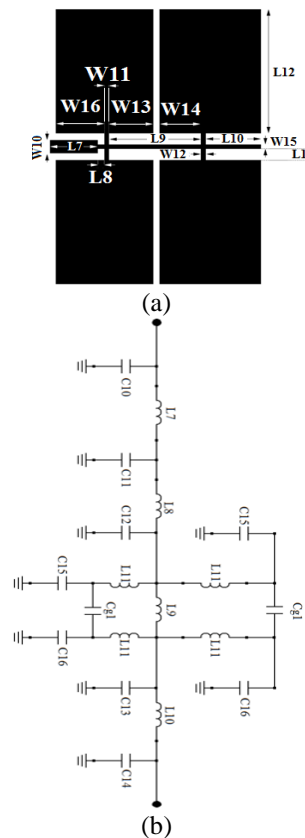


Fig. 9. (a) The configuration of suppressing cell, and (b) the equivalent LC circuit of suppressing cell.

The dimensions of the proposed suppressing cell are: $W_{10} = 0.3$, $L_{11} = 0.2$, $L_{10} = 3.2$, $L_9 = 1.25$, $L_8 = 2.1$, $L_7 = 1$, $W_{16} = 1.1$, $W_{15} = 0.1$, $W_{14} = 0.95$, $W_{13} = 1$, $W_{12} = 0.1$, $W_{11} = 0.1$ (all in millimeter), and the values of capacitances and inductors are as: $L_7 = 0.48$ nH, $L_8 = 0.132$ nH, $L_9 = 1.39$ nH, $L_{10} = 0.833$ nH, $L_{11} = 0.2$ nH, $C_{10} = 17$ fF, $C_{11} = 20$ fF, $C_{12} = 32$ fF, $C_{13} = 44$ fF, $C_{14} = 15$ fF, $C_{15} = 0.332$ pF, $C_{16} = 0.35$ pF, $C_{g1} = 75$ fF. Figure 10 depicts the results of EM simulation and the frequency response of LC circuit, which are in good agreement. As it is observed, the designed suppressing cell creates two transmission zeros (TZs) at 9.1 and 20 GHz with corresponding attenuation levels of -56 and -64 dB, respectively. These TZs have created a wide stopband from 9 up to 23 GHz with a corresponding suppressing level of -20.5 dB. Finally, by connecting two out of this suppressing cells in the both side of the combination of the resonator and S-CCRCs a LPF with -3 dB cut-off frequency of 2.4 GHz is proposed. In Fig. 11, the configuration of the proposed LPF has been shown. The remained dimensions are as follows: $L_f = 1.6$, $W_f = 1.56$, $S_5 = 0.15$ and $S_6 = 0.2$ (all in millimeter). As the previous steps, the equivalent LC circuit of the proposed LPF and its frequency response are shown in Figs. 12 (a) and (b). The values of inductors and capacitors are as follows: $L_2 = 3.4$ nH, $L_3 = 0.75$ nH, $L_5 = 2.45$ nH, $L_6 = 0.3$ nH, $L_7 = 0.48$ nH, $L_8 = 0.132$ nH, $L_9 = 1.39$ nH, $L_{11} = 0.2$ nH, $L_{12} = 2.37$ nH, $L_{13} = 3.84$ nH, $C_3 = 63$ fF, $C_4 = 0.29$ pF, $C_5 = 0.28$ pF, $C_8 = 63$ fF, $C_9 = 0.32$ pF, $C_{10} = 17$ fF, $C_{11} = 20$ fF, $C_{12} = 32$ fF, $C_{15} = 0.332$ pF, $C_{16} = 0.35$ pF, $C_{g1} = 75$ fF, $C_{17} = 72$ fF, $C_{18} = 157$ fF, $C_{19} = 180$ fF, $C_{g1} = 75$ fF, $C_{g2} = 10$ fF, $C_{g3} = 25$ fF. The frequency response of LC circuit of the proposed LPF and EM simulation are shown in Fig. 12 (b) and good agreement between them is clearly observed.

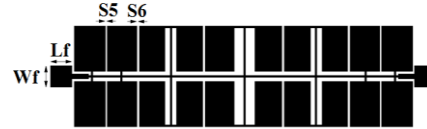


Fig. 11. The configuration of the proposed LPF.

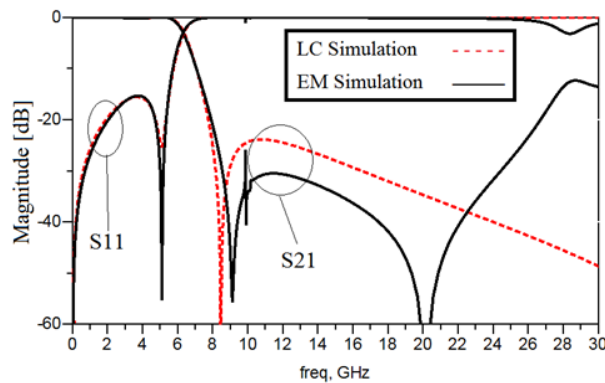
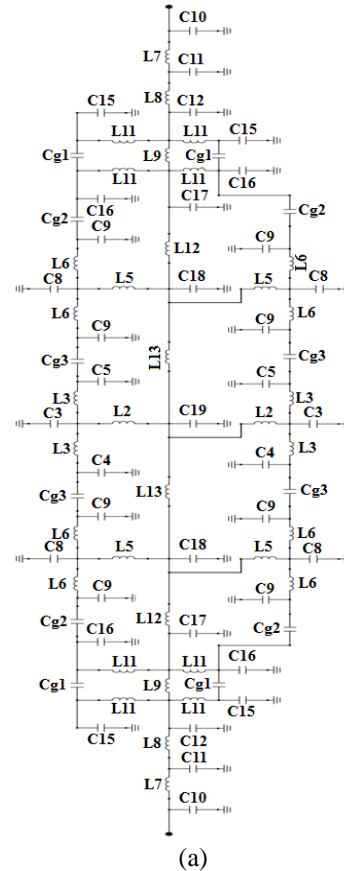


Fig. 10. EM simulation and the frequency response of LC circuit of the mentioned cells in Fig. 9.

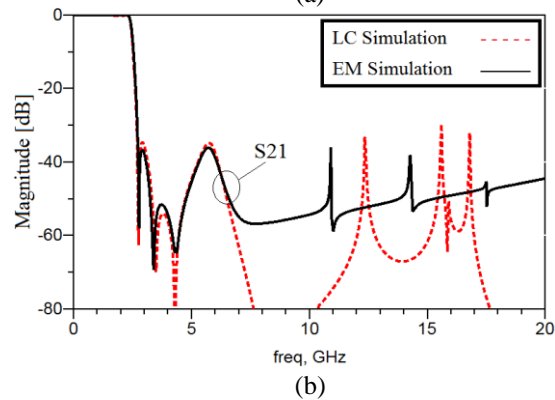


Fig. 12. (a) The equivalent LC circuit of the proposed LPF, and (b) EM and LC simulation of the proposed LPF.

III. MEASUREMENT AND SIMULATION RESULTS

The photograph of the proposed LPF is illustrated in Fig. 13. The proposed LPF has been designed, fabricated and tested. The implemented LPF has been constructed on RT/Duroid 5880 substrate with the thickness of 0.508 mm, the permittivity of 2.2 and the loss tangent of 0.0009. The simulation and measurement results of the designed LPF have been carried out by using an EM-simulator ADS based on the method of moments and a Rohde & Schwarz network analyzer ZVL13, respectively. Figure 14 shows the simulated and measured frequency responses of the proposed LPF. As it can be seen, -3 dB cut-off frequency of the filter has been located on 2.4 GHz. In the whole passband region the insertion loss is close to zero, which shows a flat response and also in this band the return loss is better than +35 dB. As it is observed, close to the operating frequency two transmission zeros (TZs) with attenuation levels of -50 and -60 are existed causing a sharp roll-off rate. Thanks to these TZs, a steep transition band about 0.27 GHz from 2.4 up to 2.67 GHz with corresponding attenuation levels of -3 and -40 dB, respectively, has been measured, which verify a desired skirt performance. The stopband region suppress spurious frequencies from 2.66 up to 23 GHz with corresponding rejection level of -35 dB. Moreover, in the rejection band a flat return loss close to zero has been obtained.

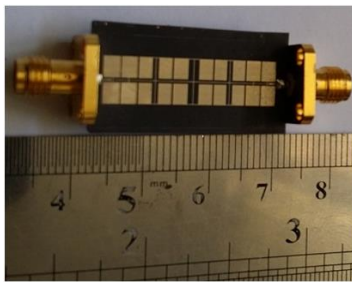


Fig. 13. The photograph of the proposed LPF.

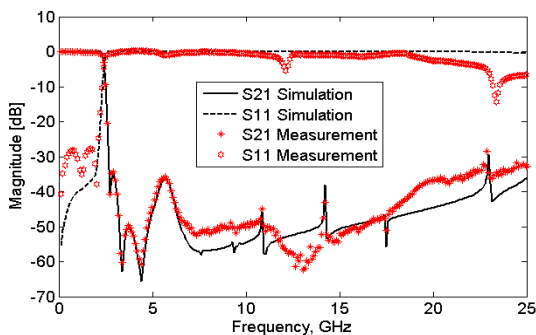


Fig. 14. The simulation and measurement results of the proposed LPF.

The occupied area of the proposed LPF is 25.5 mm \times 7.1 mm. The simulation and measurement results are in good agreement, as it was expected. For comparison, Table 1 summarizes the performance of some published lowpass filters. In this table, the roll-off rate ξ is defined as:

$$\xi = \frac{\alpha_{\max} - \alpha_{\min}}{f_s - f_c} \quad (\text{dB/GHz}), \quad (1)$$

where α_{\max} is the 40 dB attenuation point, α_{\min} is the 3 dB attenuation point, f_s is the 40 dB stopband frequency, and f_c is the 3 dB Cut-off frequency. The relative stopband bandwidth (RSB) is given by:

$$\text{RSB} = \frac{\text{stop-band bandwidth } (-20\text{dB})}{\text{stop-band center frequency}}. \quad (2)$$

The suppression factor (SF) is based on the SBW; for example, when the SBW is referred to 30 dB suppression, the corresponding SF is defined as 3. The normalized circuit size (NCS) can be derived as below:

$$\text{NCS} = \frac{\text{physical size (length} \times \text{width)}}{\lambda_g^2}. \quad (3)$$

Finally, the figure-of-merit (FOM), the overall index of a proposed filter, is given by:

$$\text{FOM} = \frac{\xi \times \text{RSB} \times \text{SF}}{\text{NCS} \times \text{AF}}. \quad (4)$$

Table 1: Comparison between the performance of the proposed lowpass filter and previous works

Ref.	Roll-off Rate (ξ)	RSB	SF	NCS	AF	FOM
[1]	36.3	1.323	1.5	0.0062	1	11543
[2]	37	1.15	2	0.021	1	3999
[3]	30	1.25	1.5	0.0064	1	8789
[4]	74	1.19	2	0.0119	1	14713
[5]	95	1.4	2	0.0222	1	11951
[6]	130	0.933	2	0.0202	2	6004
[7]	200	1.36	2	0.2995	1	1815.9
[8]	82	1.28	2.5	0.0242	1	10842
[9]	37	1.65	1.5	0.0101	1	9065
This Work	132	1.59	3.5	0.0152	1	48327

IV. CONCLUSION

In this article, by employing high-low impedance transmission lines, LC tank patches are designed to propose a LPF resonator. By connecting three of these resonators with different dimension in series, a sharp transition band has been obtained. To achieve a wide stopband eight suppressing cells are adopted. Combining the tripled resonators connected in series

and suppressing cells leads to implementing a LPF with sharp skirt performance and wide rejection band. The fabricated LPF has -3 dB cut-off frequency of 2.4 GHz.

REFERENCES

- [1] J. Wang, L.-J. Xu, S. Zhao, Y.-X. Guo, and W. Wu, "Compact quasi-elliptic microstrip lowpass filter with wide stopband," *IEE Electron. Lett.*, vol. 46, no. 20, pp. 1384-1385, 2010.
- [2] S. Luo, L. Zhu, and S. Sun, "Stopband-expanded low-pass filters using microstrip coupled-line hairpin units," *IEEE Microw. Wireless Compon. Lett.*, vol. 18, no. 8, pp. 506-508, Aug. 2008.
- [3] X. B. Wei, P. Wang, M. Q. Liu, and Y. Shi, "Compact wide-stopband lowpass filter using stepped impedance hairpin resonator with radial stubs," *IEE Electron. Lett.*, vol. 47, no. 15, pp. 862-863, July 2011.
- [4] L. Li, Z.-F. Li, and J.-F. Mao, "Compact lowpass filters with sharp and expanded stopband using stepped impedance hairpin units," *IEEE Microw. Wireless Compon. Lett.*, vol. 20, no. 6, pp. 310-312, June 2010.
- [5] V. K. Velidi and S. Sanyal, "Sharp roll-off lowpass filter with wide stopband using stub-loaded coupled-line hairpin unit," *IEEE Microw. Wireless Compon. Lett.*, vol. 21, no. 6, pp. 301-303, June 2011.
- [6] M. K. Mandal, P. Mondal, S. Sanyal, and A. Chakrabarty, "Low insertion-loss, sharp rejection and compact microstrip lowpass filter," *IEEE Microw. Wireless Compon. Lett.*, vol. 16, no. 11, pp. 600-602, 2006.
- [7] R. Gomez-Garcia, M. A. Sanchez-Soriano, M. Sanchez Renedo, G. Torregrosa-Penalva, and E. Bronchalo, "Extended-stopband microstrip lowpass filter using rat-race directional couplers," *Electron. Lett.*, vol. 49, no. 4, pp. 272-274, 2013.
- [8] C.-J. Wang and C.-H. Lin, "Compact lowpass filter with sharp transition knee by utilising a quasi- π -slot resonator and open stubs," *IET Microw. Antennas Propag.*, vol. 4, no. 4, pp. 512-517, 2010.
- [9] J. Wang, H. Cui, and G. Zhang, "Design of compact microstrip lowpass filter with ultra-wide stopband," *IEE Electron. Lett.*, vol. 48, no. 14, pp. 854-856, July 2012.
- [10] J. S. Hong and M. J. Lancaster, *Microstrip Filters for RF/Microwave Applications*. John Wiley & Sons, Inc., 2001.



Ali Reza Nouritabar received the B.S. in Electronics Engineering, from Islamic Azad University, Kermanshah Branch, Kermanshah, Iran, in 2009 and M.S. degree from the K. N. Toosi University of Technology, Tehran, Iran, in 2012. His research interests include Microwave and millimeter wave devices and circuits.



Ashkan Abdipour received the B.S. in Electronics Engineering, from Islamic Azad University, Kermanshah Branch, Kermanshah, Iran, in 2009 and M.S. degree from the Razi University, Kermanshah, Iran, in 2013. His research interests include Microwave and millimeter

wave devices and circuits.



Arash Abdipour received the B.S. in Electronics Engineering, from Islamic Azad University, Kermanshah Branch, Kermanshah, Iran, in 2009 and M.S. degree in Electronic Eng. at University of Science and Research, Kermanshah Branch, Kermanshah, Iran. His research interests include Microwave and millimeter wave devices and circuits.